Chemical Torque in $Y_{14}Ag_{39.3}Zn_{12.1}$: Unwinding the Disordered Triangles of the $Gd_{14}Ag_{51}$ Type

Rie T. Fredrickson* and Daniel C. Fredrickson*

Department of Chemistry, University of Wisconsin-Madison, 1101 University Avenue, Madison, Wisconsin 53706, United States

ABSTRACT: Elemental substitution is commonly used in materials chemistry to tune the Fermi energy of a compound or impart chemical pressure on atomic environments. In this Article, we illustrate how such substitution can also allow one to tune the relative orientations of geometrical units within a crystal structure, using the $Gd_{14}Ag_{51}$ structure type as a demonstration. A key feature of this structure type is the presence of hexagonal columns based on the $CaPd_{5+x}$ structure type, containing triangles of atoms disordered over two orientations. Synthesis and structure solution of a Zn-substituted variant of this structure, $Y_{14}Ag_{39.3}Zn_{12.1}$, reveals that the incorporation of Zn atoms into these triangles leads to a rotation of them relative to their surroundings. Distinct triangle orientations are found depending on whether they are Ag_3 or Zn_3 units. A DFT-Chemical Pressure (CP) analysis of the unsubstituted parent compound $Y_{14}Ag_{51}$ elucidates these observations. The Ag_3 triangles lie within a large hexagon of Y atoms, with each triangle corner being able to gain close contacts with up to two of these Y atoms, depending on the orientation. Obtaining an optimal alignment of the Ag_3 triangles with respect to these interactions, however, is prevented by repulsion from other Ag atoms in the columns derived from the $CaPd_{5+x}$ type. Instead, the triangles are twisted toward the Y neighbors with the larger negative CP features. The replacement of Ag atoms with smaller Zn ones provides the opportunity to relieve these packing tensions, allowing the triangles to turn to a position that optimizes their interactions with the surrounding Y atoms. These results point to simple guidelines for identifying, with CP analysis, rigid units within structures that may be manipulated through elemental substitution.

1. INTRODUCTION

Our fundamental models for metallic materials are antithetical to the existence of molecular units within them, involving delocalized electrons that collectively stabilize certain arrangements of ion cores or the packing of spheres that seek to maximize the density. However, the crystal structures of intermetallic phases are rich in geometrical features suggestive of cohesive units of atoms. For example, a variety of structures contain disordered regions in which different polyhedral units or the same units in different orientations are randomly distributed over the cells. Such occurs in Tsai-type quasicrystals and their approximants, whose basic clusters are centered by a disordered tetrahedron enclosed in a pentagonal dodecahedron,[1-5] resembling in someways the situation in endohedral fullerenes.[6,7] Similarly, the high-temperature form of Al_3Mg_2, with its 1169 atom giant cubic cell, contains disordered domains partially occupied by Friauf polyhedra and μ-phase polyhedra in different orientations; these units adopt an ordered pattern in the low-temperature form.[8-10] The ability to influence the orientational freedom and disorder of such loosely constrained polyhedral units could allow for the tuning of vibrational properties or order-disorder phase transitions.

In our explorations of the complexity in the Y-Ag-Zn system,[11] we encountered a new phase with clues to how such structural control can be attained through elemental substitution: $Y_{14}Ag_{39.3}Zn_{12.1}$. This compound represents a Zn-substituted variant of the $Gd_{14}Ag_{51}$-type phase $Y_{14}Ag_{51}$.[12] The original $Gd_{14}Ag_{51}$ type[12-15] (Figure 1) consists of a hexagonal array of columns derived from the $CaCu_5$ type[16] separated by trigonal tubes extracted from the $EuMg_5$ type.[17,18] Of particular interest is the former motif. Here, the usual array of cation-centered double hexagonal antiprisms in the $CaCu_5$ type is interrupted in by the Chemical Pressure (CP)-driven[19] periodic replacement of hexagons by Ag_3 triangles, as in the $CaPd_{5+x}$ type.[20] These Ag triangles are disordered over two orientations, related by a 60° rotation.

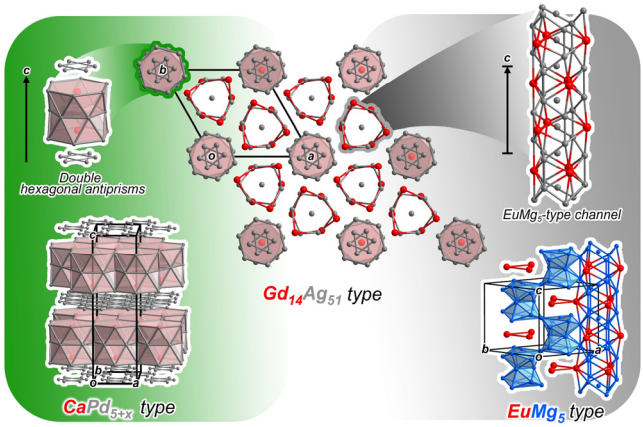

Figure 1. The $Gd_{14}Ag_{51}$ structure type, viewed as a rod packing of columns derived from the $CaPd_{5+x}$ and $EuMg_5$ types. Two major units are columns of double hexagonal antiprisms separated by disordered triangles (reminiscent of the $CaPd_{5+x}$ type, itself a derivative of the $CaCu_5$ type) and $EuMg_5$-type channels with an ordered occupation pattern.

The $Gd_{14}Ag_{51}$ type offers a wealth of structural and physical phenomena. Structurally, the type supports a number of ternary substitutions with noticeable site preferences.[21,22] In addition, positional

disorder can extend beyond the problematic triangles,[22-24] while Hg-based compounds based on this structure type can exhibit superstructures (quite complex in the case of $Na_{11}Hg_{52}$) with ordered triangle orientations.[25-27] In terms of properties, the $Gd_{14}Ag_{51}$ type's three symmetry-distinct lanthanide positions, two of which create triangular units, together with their tendency for antiferromagnetic coupling, sets the stage for magnetic frustration. Antiferromagnetic ordering can involve all or a subset of the lanthanide sites and complex magnetic structures.[12,28-30] Antiferromagnetism may also coexist with heavy Fermion effects,[28,31,32] while superconductivity has been observed in a Ge-substituted variant of $Y_{14}Au_{51}$.[33]

In this Article, we will see that the disordered triangles characteristic of this structure type can be influenced through the incorporation of Zn (an element that, to the best of our knowledge, has not significantly explored in previous substitution efforts) into the structure. DFT-Chemical Pressure analysis[34-37] of the $Y_{14}Ag_{51}$ parent phase will reveal that the packing situation for the triangles makes them effectively rigid units,[38,39] whose orientations are subject to a chemical torque arising from the competition between a driving force for stronger Y-Ag interactions and repulsion at Ag-Ag contacts. The substitution of Ag atoms with smaller Zn ones provides the opportunity to soothe this tension. Indeed, the experimental structure shows a clear rotational offset between Ag_3 triangles and Zn_3 triangles. In this way, $Y_{14}Ag_{39.3}Zn_{12.1}$ illustrates how CP analysis can reveal geometrical motifs within solid state structures whose orientations may be influenced through elemental substitutions.

2. EXPERIMENTAL

2.1. Synthesis. In our synthetic investigation of the Y-Ag-Zn, Y (Strem chemicals, 99.9%), Ag (Aldrich, 99.99%) and Zn (Alfa Aesar, 99.9%) were used as starting materials. In the synthesis of $Y_{14}Ag_{39.3}Zn_{12.1}$, the elements were weighed out in the molar ratio of Y:Ag:Zn = 14:35:16 in an Ar-filled glove box. The materials were pressed into pellets and then placed into a fused silica tube under Ar, which was then evacuated and sealed. The sample was annealed at 1100 °C for 24 hours to drive the reaction among the elements, then cooled to 500 °C, annealed there for 144 hours, and finally quenched in the ice water. After the structure of $Y_{14}Ag_{39.3}Zn_{12.1}$ was determined, we attempted its synthesis from a stoichiometric combination of elements. However, a multi-phase sample was obtained, perhaps reflecting the difficulty of reaching equilibrium in this system due to the emergence of modular intergrowth structures.[11]

2.2. Powder X-ray Diffraction Analysis. The phase composition of the sample was assessed using powder X-ray diffraction analysis. Each sample was ground to a fine powder and spread on a zero-background plate. Diffraction intensities were measured on a Bruker D8 Advance Powder Diffractometer fitted with an LYNXEYE detector, using Cu Kα radiation (λ=1.5418 Å) at ambient temperature. The exposure time of 1.0 s per 0.010° increment was used over the 2θ range of 20–80°.

2.3. Single Crystal X-ray Diffraction Analysis. Single crystal X-ray diffraction data for crystals selected from the reaction products was collected on an Oxford Diffraction Xcalibur E diffractometer using graphite monochromatized Mo Kα radiation (λ=0.7173 Å) at ambient temperature. The collection and integration of the data set were performed using the CrysAlisPro, v.171.37.35 software, as well as the SCALE3 ABSPACK module for the multiscan absorption correction. The structures were solved with the charge flipping algorithm[40,41] using the program SUPERFLIP[42] and refined on F^2 with JANA2020.[43] Further details regarding the refinements and crystallographic information are given in Table 1, as well as in Section S1 in the Supporting Information.

Table 1. Crystallographic Data for $Y_{14}Ag_{39.3}Zn_{12.1}$

Chemical formula	$Y_{14}Ag_{39.3(4)}Zn_{12.1(4)}$
WDS composition	$Y_{14}Ag_{38.4(5)}Zn_{12.3(2)}$
a (Å),	12.4958(3)
c (Å)	9.1520(3)
Volume (basic cell, Å^3)	1237.58(6)
Z	1
Space group	*P6/m*
Crystal dimensions (mm^3)	0.085 × 0.053 × 0.015
Crystal color, habit	Silver, prismatic
Data collection temperature	Ambient
Radiation source, λ (Å)	Mo Kα sealed tube, 0.71073
Absorption correction	Multi-scan
Min/max transmission	0.5463/1.000
θ_{min}, θ_{max}	2.91/28.85
Refinement method	F^2
Number of reflections	10175
Unique refl. [I > 3σ(I), all]	1095
R_{int} [I > 3σ(I), all]	7.33, 8.41
Number of parameters, constraints	67, 33
R[I > 3σ(I)], R_w[I > 3σ(I)]	3.48, 5.78
R(all), R_w(all)	6.31, 6.63
S[I > 3σ(I)], S(all)	1.10, 1.14
$\Delta\rho_{max}$, $\Delta\rho_{min}$(electrons/Å^3)	2.84, -3.76

2.4. Wavelength Dispersive X-ray Spectroscopy. To determine the elemental compositions of the phases synthesized, wavelength dispersive X-ray spectroscopy (WDS) was performed for a sample from which single crystals of $Y_{14}Ag_{39.3}Zn_{12.1}$ were obtained and whose powder X-ray diffraction pattern suggested the presence of this phase. A small amount of material was suspended in a conductive epoxy at one end of a short segment of aluminum tubing. Once the epoxy had hardened, the sample was ground to produce a flat surface and then polished using a diamond lapping film (Precision Surface International Inc., 0.5 μm). Finally, the sample was carbon coated. WDS measurements guided by back-scattered electron (BSE) images were taken with a Cameca SX-Five FE-EPMA Microprobe, using Y_2O_3, elemental Ag, elemental Zn, and elemental Si, as standards for Y Lα, Ag Kα, Zn Kα, and Si Kα, respectively. The individual data points from the WDS measurements are provided in Section S2 of the Supporting Information.

2.5. DFT-Chemical Pressure Analysis. DFT-Chemical Pressure (CP) schemes[34-37] were calculated for an ordered model of $Gd_{14}Ag_{51}$-type $Y_{14}Ag_{51}$ using the output of LDA-DFT calculations carried out with the ABINIT package.[44,45] The energy cutoff was set to 50 Ha, while a 3×3×5 Γ-centered k-point mesh and Hartwigsen-Goedecker-Hutter norm-conserving pseudopotentials[46] were employed. First, the structure of $Y_{14}Ag_{51}$ was geometrically optimized, beginning with the relaxation of the atomic positions within a fixed unit cell and then including also the cell parameters. Single point calculations were then carried out on the ground state structure as well as slightly expanded and contracted versions (linear scale ±0.5 %) to obtain the electron densities, Kohn-Sham potential compounds, wavefunctions, and kinetic energy densities needed for the construction of CP maps. The optimized geometrical parameters, as well as electronic density of states distribution, are provided in Section S3 of the Supporting Information.

CP maps were then generated with the DFT-CP package, using the core unwarping procedure,[47] the iterative binary Hirshfeld scheme for the partitioning of space among atoms and interatomic contacts,[37] and the self-consistent treatment of the E_{Ewald}+E_{α} contributions to the pressure maps.[48] The CP maps were then interpreted in terms of interatomic interactions using the iterative binary Hirshfeld contact volume scheme[45,48,49] (with the Atomic Pseudopotentials Engine[48] being called for the necessary free atom calculations), with interatomic pressures being projected onto atomic-centered spherical harmonics (l_{max} = 4 for visualzation). The CP schemes were plotted with an in-house MATLAB application, figuretool. CP schemes were also generated for variants of the $Y_{14}Ag_{51}$ structure in which the orientation of the Ag triangle subject to disorder is turned in two different directions (without re-optimization of the structure).

3. RESULTS AND DISCUSSION

3.1. Synthetic results. In our prior exploration of modular structures in Y-Ag-Zn, we repeatedly encountered a $Gd_{14}Ag_{51}$-type phase using different molar ratios in Zn- and Ag- rich sides. Our solid state reaction targeting this phase yielded metallic silver-colored, air-stable ingots, which were brittle and easily crushed with a hammer into smaller pieces. Shiny prismatic crystals were selected from the sample for use in single crystal X-ray diffraction measurements. The remainder of the fragments were ground in an agate mortar for powder X-ray diffraction measurements or imbedded in epoxy and polished to yield flat surfaces for wavelength dispersive X-ray spectroscopy (WDS) measurements.

The powder X-ray diffraction pattern revealed a complicated series of peaks (black, top box in Figure 2a), some of which can be assigned to a $Gd_{14}Ag_{51}$-type phase (blue). However, there are additional peaks, some of which can be indexed with a $EuMg_5$-type phase related to YZn_{5+x}[50] or a $CaCu_5$-type phase. The clues to the origins of the remaining peaks are provided by a phase analysis performed with scanning electron microscopy back scattered electron (SEM-BSE) imaging, coupled with WDS measurements. The SEM-BSE imaging (Figure 2b) reveals a multi-phase distribution, with four different phases labeled as bright, medium bright, medium, and dark. As the maximum number of thermodynamic phases for a ternary system is 3, it appears that at least one metastable phase has been trapped, with multiple phases being in competition at Y:(Ag/Zn) ratios near 1:5.

The WDS composition for the medium bright phase is $Y_{21.6(2)}Ag_{59.3(3)}Zn_{19.1(2)}$ (20 measurement points, normalized composition$Y_{14}Ag_{38.4(5)}Zn_{12.4(2)}$) aligns with that expected for a $Gd_{14}Ag_{51}$-type phase, and in fact matches (within 3σ) the composition refined from single crystal X-ray diffraction data, $Y_{14}Ag_{39.3}Zn_{12.1}$. The WDS measurements for the remaining three phases yielded compositions of $Y_{16.2(7)}Ag_{58.5(3)}Zn_{25.3(9)}$ (11 measurement points, medium phase), $Y_{16.9(2)}Ag_{57.5(2)}Zn_{25.6(2)}$ (20 measurement points, dark phase), and $Ag_{76.9(2)}Zn_{23.1(2)}$ (20 measurement points, bright phase). Based on comparison with powder diffraction data, the first two of these phases (medium and dark) are likely Ag-substituted variants of YZn_{5+x}[50] or the $CaCu_5$ type, while the third is likely a simple Ag/Zn fcc alloy.[51]

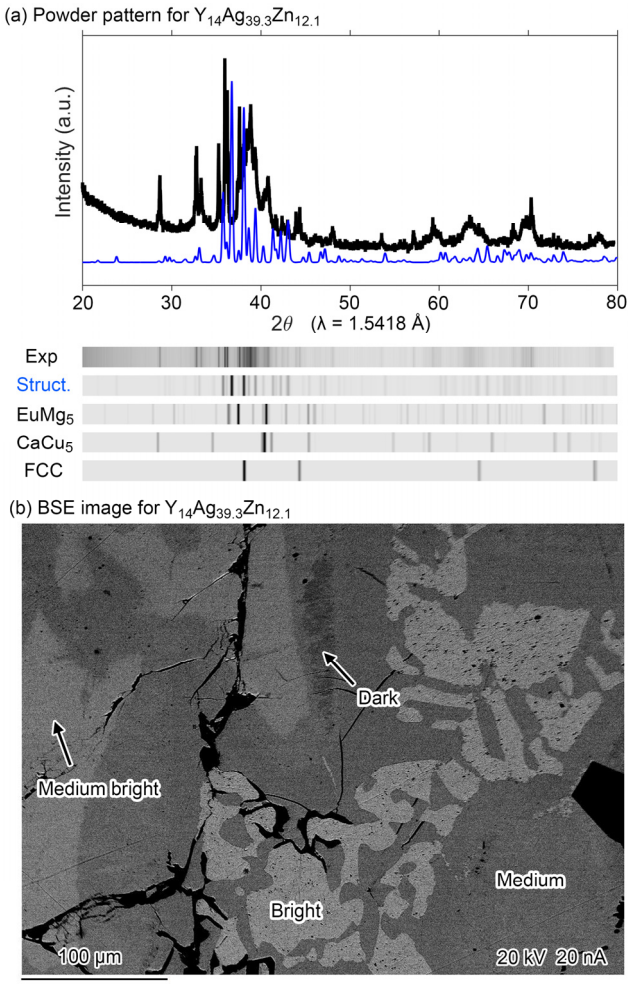

Figure 2. Phase analysis for sample containing the $Gd_{14}Ag_{51}$-type phase $Y_{14}Ag_{39.3}Zn_{12.1}$. (a) Powder X-ray diffraction pattern, with the calculated pattern from the refined structure shown with blue bars. A film-strip-style representations of the experimental pattern is shown below along with simulationed patterns for $Y_{14}Ag_{39.3}Zn_{12.1}$, $EuMg_5$-type YZn_5, $CaCu_5$-type YZn_5, and fcc-Ag. (b) SEM back-scattered electron (BSE) image of polished sample, showing contrast between regions with different compositions; see the text for the WDS compositions for the phases labeled.

3.2. Structure solution and refinement. The diffraction pattern of a single crystal picked from the Y-Ag-Zn product was indexable with a hexagonal unit cell with a=12.50 Å, c=9.15 Å (Table 1), with the Laue symmetry being consistent with the $Gd_{14}Ag_{51}$ type's space

group, *P6/m*. The structure solution was performed with the charge-flipping algorithm confirmed the symmetry and structure type, while the refinement process easily converged on the basic framework of the structure, with many of the sites showing Ag/Zn mixed occupancy.

The main challenge from the crystallographic point of view is the modeling of the structure type's disordered region, where triangles with different orientations appear overlaid. An (*x,y*) cross-section through the Fourier electron density map for a *P*1 refinement exhibits six elongated ellipsoidal features tracing out a hexagon. None of these features has sufficient electron population for full occupancy, suggesting either disorder or the possibility of the superposition of twin domains. We tested twinned models in hexagonal, trigonal or orthorhombic cells, but the structure agreement factors were either too high or the refined chemical composition did not agree with the WDS analysis results.

The refinement proceeds much more smoothly considering the structure as disordered in the *P6/m* space group. We began by modelling each peak in the density as a mixed Ag1/Zn1 position assuming 50% total occupation, corresponding to two triangles rotated from each other by 60° around the *c*-axis. The unsatisfactory agreement with the data then led us to refine partial occupancies for Ag1 and Zn1 separately and allow independent atomic coordinates for Ag1 and Zn1. The result was a significant split between the Ag1 and Zn1 positions (Figure 3), with the sum of refined occupancies for Ag1 and Zn1 sites being a little higher than the expected 50%, with occ(Ag1)=22.3% and occ(Zn1)=33.9% (perhaps reflecting some Ag incorporation at the Zn1 site not accounted for in our model). The refined composition of the final model is $Y_{14}Ag_{39.3}Zn_{12.1}$, which is within the range of 3σ for the WDS composition of $Y_{14}Ag_{38.4(5)}Zn_{12.3(2)}$. The refined atomic coordinates are given in Table S1, while the atomic displacement parameters are listed in Table S2. An examination of the interatomic distances (Table S3) reveals that the Y-Ag, Y-Zn, and Ag-Zn distances are near the expected ranges of approximately 2.8 to 3.5 Å, 2.75 to 3.6 Å, and 2.6 to 3.0 Å, respectively, as judged from histograms of such contacts in the Inorganic Crystal Structure Database (ICSD).[52,53]

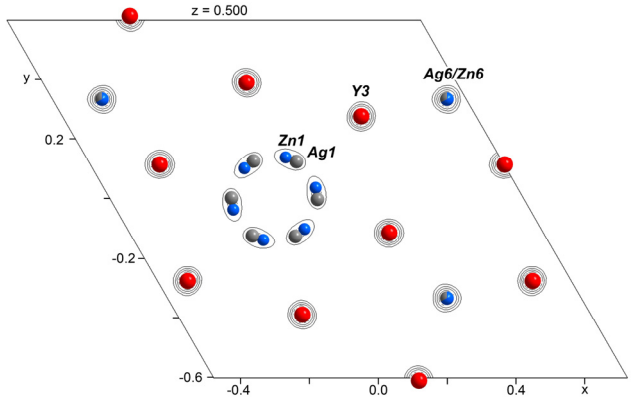

Figure 3. Cross-section (x,y) of the $Y_{14}Ag_{39.3}Zn_{12.1}$ Fourier electron density through the disordered region (z=1/2). The elongated density features are modeled with the partially occupied split Ag1/Zn1 sites.

3.3. Interpretation of the $Y_{14}Ag_{39.3}Zn_{12.1}$ structure: atomic site preferences. The refined structure $Y_{14}Ag_{39.3}Zn_{12.1}$ represents a variant of the $Gd_{14}Ag_{51}$ type with intensified disorder. An overview of this structure is shown in Figure 4, with the major building units emphasized. Columns based on the $CaPd_{5+x}$ type, with Y atoms hosted in Ag/Zn double hexagonal antiprisms (pink) separated by disordered Ag or Zn triangles, propagate along the *c*-direction. These hexagonal columns are surrounded by $EuMg_5$-type channels (yellow).

Throughout this framework, the Ag and Zn exhibit varying degrees of mixing, suggestive of noticeable site preferences as observed in Ln-Au-M (Ln = Y or lanthanide, M = p-block element) $Gd_{14}Ag_{51}$-type phases.[22] Within the double hexagonal antiprisms derived from the $CaPd_{5-x}$ type, the upper and lower hexagons (green, derived from honeycomb layers in the $CaPd_{5+x}$ type) show higher Ag content, with the refined ratio for the Ag3/Zn3 site being 84% Ag, 16% Zn. Meanwhile, the central hexagon (blue, corresponding to a kagome net in the full $CaPd_{5-x}$ type) shows a higher preference for Zn, with the refined composition for the Ag4/Zn4 site being 45% Ag and 55% Zn.

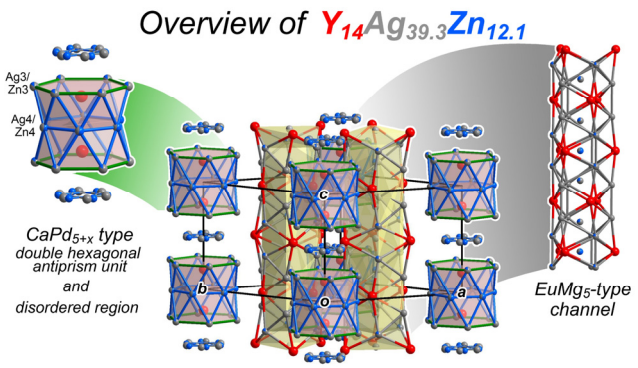

Figure 4. The crystal structure of $Y_{14}Ag_{39.3}Zn_{12.1}$, with mixed Ag/Zn occupancies shown. $CaPd_{5+x}$ type columns with hexagonal antiprisms (pink) hosted Y atoms (red) are surrounded by $EuMg_5$ type channels (yellow).

The disordered trigonal region also shows a relatively high affinity for Zn; the Zn1 occupation is 34% compared to 22% for Ag1. Hints toward the origin of the preference here can be discerned in the patterns made by the sites. As shown in Figure 5, the partial occupancies can be interpreted in terms of the superposition of two triangle units for both the Ag1 and Zn1 sites, creating a total of four distinct triangle orientations (triangles constructing from combinations of Zn1 and Ag1 positions inevitably contain unphysically short distances). The Zn1- and Ag1-based triangles are surrounded by Y atoms from the $EuMg_5$ type channel walls and aligned differently with respect to the Ag3/Zn3 hexagons above and below (Figure 5a). The corners of either $(Zn1)_3$ triangle unit point directly towards hexagon corners in the projection down **c** (Figures 5b, c), while the $(Ag1)_3$ triangles (Figure 5d, e) triangle are tilted clockwise by about 16° off of these hexagon corners. This twist significantly changes the interatomic distances, and, as we will see in Section 3.5, atomic packing tensions play a significant role in driving it.

Looking down the *c*-axis, the $EuMg_5$-type channels form a honeycomb pattern around the $CaPd_{5+x}$-type columns, connecting to the double hexagonal antiprism Ag3/Zn3 sites through contacts of 2.89 to 3.00 Å to the Ag7 sites with full Ag occupancy. The other Ag/Zn site in the $EuMg_5$ type channel walls is Ag2/Zn2 with 81% Ag, 19% Zn, while the channel is occupied by the Ag5/Zn5 and Ag6/Zn6 sites with Ag/Zn ratios of 71% Ag, 29% Zn and 33% Ag, 67% Zn, respectively.

3.4. Occupation pattern in the EuMg$_5$-type channels. EuMg$_5$-type channels such as those found in $Y_{14}Ag_{39.3}Zn_{12.1}$ are commonly observed in a range of phases in the Y-Ag-Zn system,[50] with the channel occupants showing varying degrees of ordering. They are built from an alternation of tricapped trigonal prisms and flatted octahedra linked through shared triangular faces. The centers of the tricapped trigonal prisms, the centers of the octahedra or positions near the centers of the shared triangular faces can host atoms.

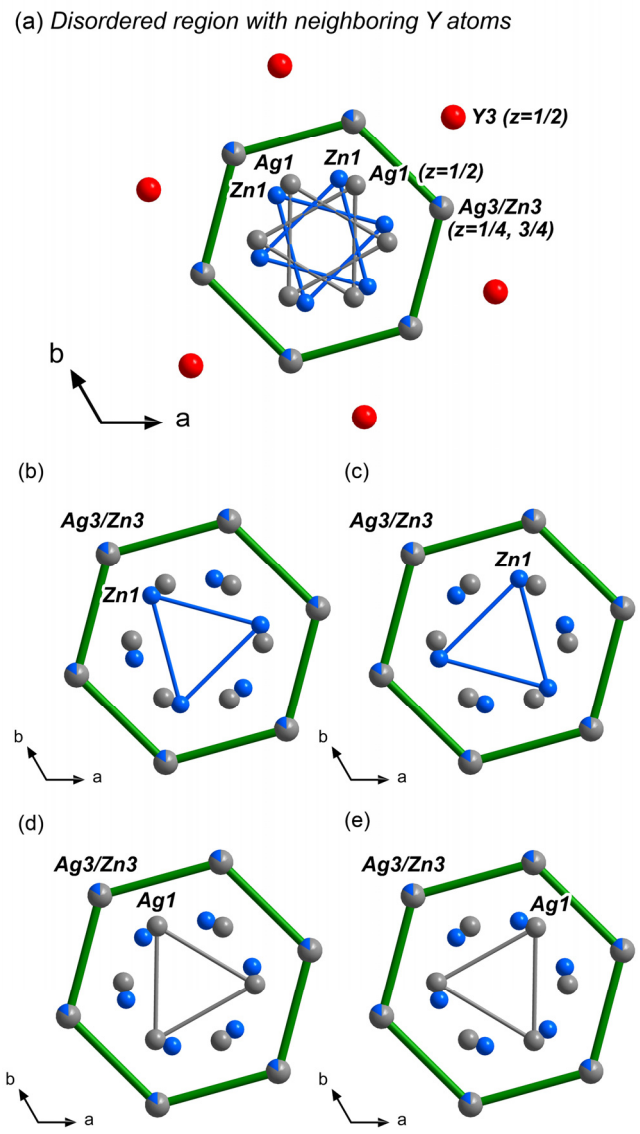

Figure 5. Disorder patterns of the split Ag1 and Zn1 sites. (a) Ag1 or Zn1 disorder region and the hexagon of Ag3/Zn3 atoms (green) are surrounded by the neighboring Y3 atoms from the EuMg$_5$-type channel wall. The disorder pattern can be interpretted in term of (b,c) Zn_3 triangles in two orientations or (d,e) corresponding Ag_3 triangles that twisted ~16° clockwise. The heights for the triangle atoms and Y atoms are z=1/2. Hexagons of Ag3/Zn3 atoms occur at heights z=1/4, 3/4.

In our earlier study in the binary Y-Zn system, we reinvestigated the EuMg$_5$-type phase YZn_5 structure, discovering that rather than a series of sparsely distanced Zn atoms (Zn-Zn distance at 4.603 Å), the channels have a disordered occupation pattern, leading to the composition YZn_{5+x} (x=0.025). Based on the paths for CP communication between neighboring channels, we proposed that an ordered $\sqrt{3}\times\sqrt{3}\times3$ superstructure could arise.[50] In fact, introducing controlled cooling step in the synthesis procedure resulted in YZn_{5+x} (x=0.017) crystals exhibiting satellite reflections corresponding to an ordered occupation pattern, locally resembling that proposed but incommensurately modulated.

Similar channels also appear in three new ternary structures we recently reported in the Y-Ag-Zn system: $YAg_{2.79}Zn_{2.80}$, $YAg_{2.44}Zn_{3.17}$, and $YAg_{2.71}Zn_{2.71}$.[11] Together, they comprise a family of the structures built from the intergrowth of Mg_2Zn_{11}- and $CaPd_{5+x}$-types domains. EuMg$_5$-type channels appear in the $CaPd_{5+x}$-types domains, with various occupation patterns. For the $YAg_{2.79}Zn_{2.80}$, the refined atomic sites in the EuMg$_5$-type channels represents a more ordered case, with the pairs of fully occupied Zn sites (triangle sites) in the channel separated along the channel by partially occupied Ag sites (tricapped trigonal prism), resulting in Zn-Zn and Ag-Zn distances of 2.681 Å and 3.145 Å, respectively. For $YAg_{2.44}Zn_{3.17}$ and $YAg_{2.71}Zn_{2.71}$ structures, the channel occupation becomes more disordered, with the Fourier density features being significantly smeared into a column for the latter case.

In the case of the structure $Y_{14}Ag_{39.3}Zn_{12.1}$ described here, the Fourier electron density map in the EuMg$_5$-type channel exhibits nearly spherical density features within the channel (Figure 6). We model them with two crystallographically distinct Ag/Zn sites. The Ag6/Zn6 sites are at the centers of every other tricapped trigonal prism along the channel, while the Ag5/Zn5 sites lie in the shared triangular faces of vacant tricapped trigonal prisms. Together, these sites mirror the occupation pattern observed for the EuMg$_5$-type channels in $YAg_{2.79}Zn_{2.80}$. This time, however, the Ag/Zn preferences are reversed. While the tricapped trigonal site is preferred by Ag in $YAg_{2.79}Zn_{2.80}$, in $Y_{14}Ag_{39.3}Zn_{12.1}$ it shows a majority Zn occupation (Ag 32.9%, Zn 67.1%). Similarly, while the triangular face site in $YAg_{2.79}Zn_{2.80}$ are strikingly preferred by Zn, in $Y_{14}Ag_{39.3}Zn_{12.1}$ they have greater Ag content (Ag 71.2%, Zn 28.8%). These different Ag/Zn ratios are reflected in the Ag5/Zn5-Ag6/Zn6 and Ag5/Zn5-Ag5/Zn5 distances of 2.6807(1) Å and 3.7906(1) Å, respectively, along the channel. The distance for Ag5/Zn5-Ag6/Zn6 falls within the typical Ag-Zn interatomic distance range, and while the longer Ag5/Zn5-Ag5/Zn5 distance is suggestive of greater population by the larger Ag atoms.

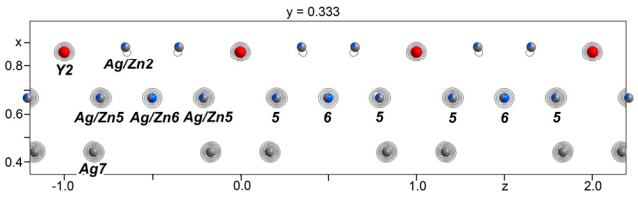

Figure 6. Fourier electron density cross section through EuMg$_5$-type channel in $Y_{14}Ag_{39.3}Zn_{12.1}$. The atomic sites associated with the channel has mixed occupancy of Ag and Zn atoms, which are labeled as Ag/Zn5 and Ag/Zn6.

3.5. DFT-Chemical Pressure analysis: triangles and Ag/Zn occupation. Driving forces for the splitting of the Ag_3 and Zn_3 triangle orientations can be discerned in the DFT-Chemical Pressure (CP) scheme of the unsubstituted parent phase, $Y_{14}Ag_{51}$. The electronic density of states distribution calculated for this compound suggests that it is metallic, with nearly-free electron states[54] at the

Fermi energy (see Section S3 in the Supporting Information). Atomic packing effects may then play a dominant role in the observed structural features. In DFT-CP analysis,[13] the output of electronic structure calculations is used explore such effects by resolving the net internal pressure of a solid state phase into contributions from different interatomic interactions. The result is a visual representation of atomic packing tensions with a compound, which in some cases can be severe enough to induce structural transformations.

In Figure 7a, we present the corresponding scheme calculated for $Y_{14}Ag_{51}$. Here the local pressure distribution experience by each atom is represented with a radial plot, with the distance from the atomic center to a point on the surface being proportional to the magnitude of the sum of the pressure contributions along that direction. The sign of the pressure is given by the color of the surface. Black lobes denote directions from which the atom experiences negative pressure (contraction of the structure, e.g. shorter interatomic distances, would be favorable). White features, on the other hand, correspond to positive pressures (where expansion of the structure, and longer interatomic distances, would be preferred).

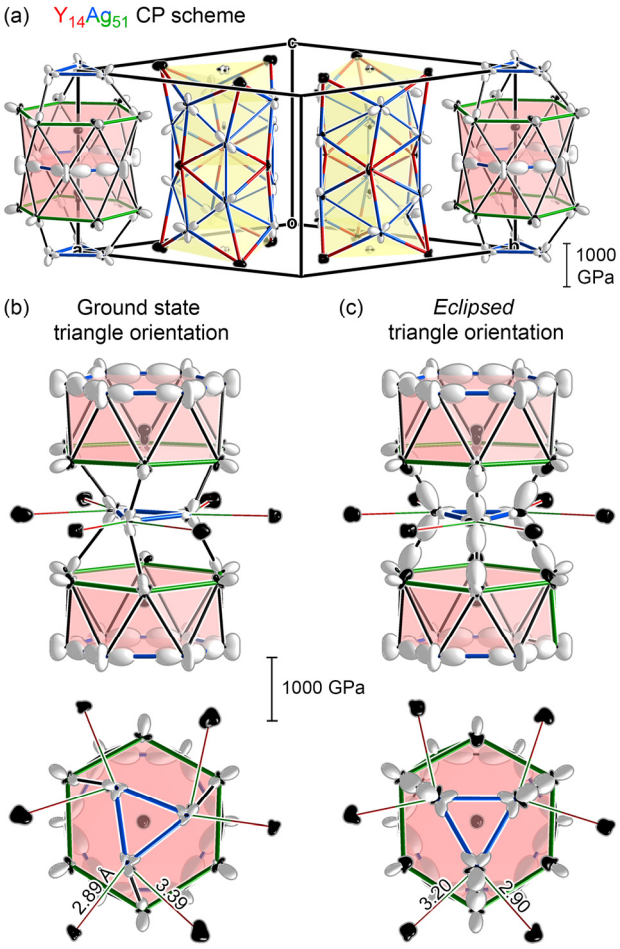

Figure 7. DFT-CP scheme for an ordered model of $Y_{14}Ag_{51}$. (a) CPs plotted for the full crystal structure. (b)-(c) Side and top views of the regions containing the Ag_3 triangles subject to disorder in the experimental structure, with the triangles placed in either (b) the ground state orientation or (c) an *eclipsed* configuration with respect to vertices of the Ag hexagons above and below it.

The Y atoms appear, both in the $CaCu_5$-type units and in the walls of the $EuMg_5$-type channels, with bulbous black surfaces representing negative pressure. These atoms would prefer tighter coordination environments in all directions. The CP features for the Ag atoms are more diverse, but a common theme is positive pressures along Ag-Ag interactions, which resist the Y atom's impetus for contraction of the structure. Most prominent are the CPs around the central hexagon of the double hexagonal antiprisms (derived from the kagome nets of the $CaCu_5$ type), as well as the contacts between these hexagons with Ag atoms on the neighboring $EuMg_5$-type columns. Altogether this CP scheme for $Y_{14}Ag_{51}$ largely reflects competition between Y-Ag (negative) and Ag-Ag (positive) CPs, a theme that is common to structures derived from the $CaCu_5$ type.[19,37,50,55]

In our previous work, we have already explored how $Gd_{14}Ag_{51}$ type can provide CP relief relative to such a $CaCu_5$ type parent structure.[19] Our focus now is on how CPs influence the disordered Ag_3 triangles in the structure. The center panels of Figure 7b provides a close-up of the CP features of one such triangle, along with its local context, viewed from the side or the top. Only a glance at the Ag-Ag interactions in this region is needed to see that the triangle leads a constrained existence. The triangle atoms are squeezed by positive CPs from Ag hexagons above and below. Motions directly away from these neighbors, however, are prevented by positive CPs within the Ag_3 triangle. These positive CPs within the triangle mean that any motion at one corner will be stiffly communicated to the other corners; the triangle is poised to make any movements collectively, as a rigid unit.

Other atoms are also acting on the Ag_3 triangles, as is best seen in the top-down view (Figure 7b, bottom). The triangle lies in the same plane with a hexagon of Y atoms (from the walls of the $EuMg_5$-type channels). Each Ag_3 corner draws near to two different Y atoms in this hexagon, with uneven distances of 2.89 Å and 3.39 Å (in the DFT-optimized structure) that reflect a twisted orientation of the triangle with respect to the edges of the hexagon. The unequal Y-Ag distances have consequences in the CP scheme. The more distance Y atoms show larger negative CP features, with the CP surface being extended in the generate direction of the triangle. Meanwhile, each of the more proximal Y atoms exhibits only minor negative CP along its contact with the triangle.

The geometry of this situation offers an easy way to solve this imbalance in the Y-Ag CPs: why doesn't the triangle simply turn to lengthen the shorter Y-Ag contacts and shorten the longer ones? The answer lies in the positive Ag-Ag CPs that we described above, as can be seen by examining the CP scheme for a such a case (Figure 7c). A turn of about 23° degrees relative to the ground state structure creates a geometry in which the triangle atoms directly align with Ag atoms in the neighboring hexagons of the double hexagonal antiprisms (which we might refer to as an *eclipsed* configuration; one can also turn them the other way to achieve a corresponding staggered configuration, as shown in Supporting Information, but little changes in terms of the CPs from the ground state structure). Performing this rotation provides substantial CP relief to the formerly distal Y atoms (with some growth of the negative CP on the ones that were strayed away from). However, the positive CPs from the triangle to the Ag atoms above and below have grown severely.

The CP distributions on the Ag_3 units in this eclipsed configuration have some telling features. Each atom has lobes that are approximately arrayed in a trigonal bipyramid, with negative lobes (Y-Ag interactions) along the axial directions and the positive lobes in the equatorial positions (two lobes pointing to Ag atoms above and below the triangle plus a positive feature that is overall directed toward the center of the triangle but somewhat bifurcated into individual Ag-Ag interactions within the ring). This arrangement of negative CP perpendicular to positive CPs creates a quadrupolar distribution, a feature associated with anisotropic atomic motions. In this case, motions that tend to turn the triangle one way or the other would tend to be soft, as they move along negative CPs without shortening contacts with positive CP. Almost any other motion would compress interactions with positive CP, and would be expected to be hard.

Based on this picture, the eclipsed configuration represents a sort of transition state between the observed ground state triangle orientation and an alternative with the triangle turned toward the other set of Y neighbors. Why is only one of these orientations observed in $Y_{14}Ag_{51}$? The CP scheme offers a reason: from the eclipsed configuration, where the Ag-Ag distances are presumably at their most strained, the two Y-Ag interactions on each triangle atom are unequal. The pull toward the experimentally observed orientation is stronger, providing a net torque on the triangle.

We are now in a position for understanding how the incorporation of Zn into the structure may influence the triangle orientations in the $Gd_{14}Ag_{51}$ type. Zn atoms, being smaller and less electronegative than Ag atoms are expected to prefer sites in the structure which exhibit more positive atomic charges and more positive net atomic CPs in our $Y_{14}Ag_{51}$ calculation. These charges and pressures are listed in Table 2, where it can be seen that the Ag1 (Ag_3 triangle) and Ag4 (kagome-derived hexagon, blue) sites would benefit most from the replacement of Ag by a smaller atom. Indeed, these represent two of the three sites with the greatest Zn occupancy (curiously, the other corresponds to the Ag5 site, located in the $EuMg_5$-type channel; we'll consider this site in Section 3.6).

Table 2. Mapping of iterative binary Hirshfeld charges and net atomic CPs calculated for $Y_{14}Ag_{51}$ to the experimental site occupancies in $Y_{14}(Ag_{1-x}Zn_x)_{51}$, x=0.24.

Site	Occupancy	ibH charges	Net CPs (GPa)
Y1	1	0.93	-165.4
Y2	1	0.99, 1.01	-131.4, -138.6
Y3	1	1.04, 1.05	-193.0, -263.7
Ag1	0.2225 Ag	-0.28	+123.6
Zn1	0.3386 Zn		
Ag2/Zn2	0.81 Ag, 0.19 Zn	-0.29, -0.28	+57.2, +76.0
Ag3/Zn3	0.84 Ag, 0.16 Zn	-0.29, -0.26	-27.9, +52.5
Ag4/Zn4	0.45 Ag, 0.55 Zn	-0.21, -0.21	+224.2, +228.5
Ag5/Zn5	0.71 Ag, 0.29 Zn	-0.24, -0.24	-0.3, +18.9
Ag6/Zn6	0.33 Ag, 0.67 Zn	-0.27, -0.25	+38.3, +51.1
Ag7	1	-0.33, -0.33	+8.5, +3.2

The placement of Zn into the triangle sites would significantly change the balance of forces acting on it. The smaller size of Zn atoms would serve to lower the positive pressures acting between them and the Ag honeycomb-derived hexagons (green) above and below, reducing the cost for the rotation of the triangle to equalize the Y-Zn distances. Indeed, in the refined crystal structure of $Y_{14}Ag_{39.3}Zn_{12.1}$, the Zn1 site (the Zn component of the split triangle position) is shows nearly equal Y-Zn distances of 3.12 Å and 3.07 Å, while the corresponding distances for the Ag1 site are 2.87 Å and 3.40 Å. A similar effect may be at work in the $Gd_{14}Ag_{51}$-type phase $Y_{14}(Au_{0.83}Ge_{0.17})_{51}$, where mixed occupancy on the disordered triangle sites coincides with elongated thermal ellipsoids.[33]

In this section, we have seen how the CP scheme of $Y_{14}Ag_{51}$ sets up the Ag_3 triangles as rigid units, which are subjected to competing driving forces to maximize Y-Ag interactions while achieving longer Ag-Ag contacts. Strong Ag-Ag positive pressures between the triangles and Ag hexagons above and below require the triangles to twist relative to positions with well-equalized Y-Ag distances, leading to unbalanced negative pressures on the Y atoms. The introduction of Zn into the structure tunes these effects, reducing the costs of equalizing the pressures on the Y atoms, and inducing the triangles to turn accordingly.

3.6. DFT-Chemical Pressure analysis: Flexible $EuMg_5$-type channels. There is another remarkable feature of the $Y_{14}Ag_{51}$'s CP scheme: the pressures that we don't see. The occupants within the $EuMg_5$-type channel in this structure experience nearly imperceptible CPs compared to those of the other sites in the structure. Why are these channel sites spared the competition for longer and shorter contacts seen elsewhere in the structure?

The CP features of the surrounding atoms in the channel walls offer an explanation (Figure 8): the Ag atoms in the channel walls exhibit positive CPs (toward each other and Ag atoms in the $CaPd_{5+x}$-

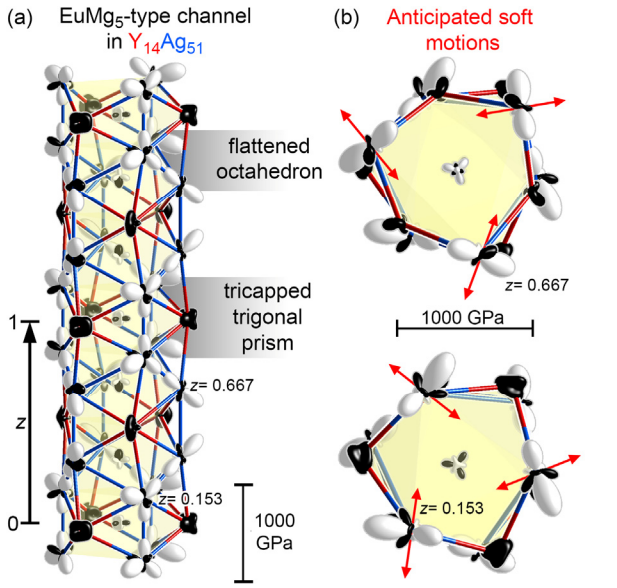

Figure 8. Quadrupolar CP features of the atoms in the walls of around $EuMg_5$-type channels of $Y_{14}Ag_{51}$. (a) Side view of one channel. (b) Top views cut at different z values, with directions of easy atomic motion anticipated by the CP features qualitatively shown in red.

type units) that run almost tangentially to the channel's circumference. Along nearly perpendicular directions, they show weak negative pressures. As for the Ag_3 units in disordered triangle region, we again encounter positive CPs running approximately perpendicular to negative ones to create quadrupolar distributions. In this case, the soft motions anticipated by the quadrupoles correspond to breathing modes of the channel walls, allowing the channel to adapt to the size requirements of the occupants (red arrows).

This feature of the channel explains how the Ag6/Zn6 site hosts a high occupation by Zn, even though the $Y_{14}Ag_{51}$ CP scheme does not show a strong driving force for the placement of a smaller atom here. When compared to the case of the Ag_3 and Zn_3 triangles, it also illustrates how the same atomic-level CP feature, a CP quadrupole, can give rise to quite distinct phenomena depending on how they are arranged in space. In the Ag_3 or Zn_3 triangles, the quadrupoles occur in clusters with their positive lobes pointing to the center, setting up soft modes for the tilting of the cluster. In the $EuMg_5$-type channels, on the other hand, the quadrupoles line the walls of a tube, with positive CPs along these walls. Now it is motions of individual atoms toward and away from the channel center that become facile.

4. CONCLUSIONS

In this Article, we have explored the potential of addressing the disordered clusters in crystal structures through elemental substitution, using the $Gd_{14}Ag_{51}$ as a model system. We began with the synthesis and structure refinement of a Zn-substituted version of $Y_{14}Ag_{51}$, $Y_{14}Ag_{39.3}Zn_{12.1.}$ In this phase, the Zn atoms are not distributed randomly over the Ag positions, but show a particular preference for certain sites, including those belonging triangles disordered over two orientations related by a 60° rotation. In this region of the structure, Zn incorporation leads to a splitting of the atomic sites corresponding to a slight rotation Zn_3 triangles relative to Ag_3 ones (which coupled to the original 60° rotational disorder gives 4 possible triangle orientations in total). DFT-Chemical Pressure (CP) analysis elucidates this behavior, revealing that in the simple binary $Y_{14}Ag_{51}$ structure the Ag_3 triangles are prevented forced to twist relative to an orientation with balanced Y-Ag interactions by positive CPs to neighboring Ag atoms. Substitution by smaller Zn atoms offers an opportunity to relieve these positive pressures, such that Zn_3 triangles can turn back into ideal alignment with their field of Y neighbors.

In understanding these factors that influence the triangle orientations, one might wonder if elemental substitution could also be used to induce ordering of the triangle positions, similar to the way that Eu incorporation in the YCd_6 quasicrystal approximant induces superstructure order.[56] A possibility is suggested by our CP scheme for $Y_{14}Ag_{51}$, which was calculated on an ordered model with all triangles oriented in the same way, bringing the space group symmetry down from *P6/m* to *P-6*. In the process, many of the atomic sites are split into two distinct sites, with potentially different chemical pressures. The Ag positions in hexagons above and below the triangles, Ag3/Zn3 are split into two sites with strikingly different pressures depending on their distance from the nearest triangle atom. One represents a rare case of a Ag atom in the structure with a negative CP, e.g. where substitution by a larger atom may be favorable. Perhaps inclusion of a small amount of, say, Cd in the synthesis of $Y_{14}Ag_{51}$ could promote ordering of the triangle orientations driving a differentiation between these positions.

We are also looking forward to investigating how the notion of CP-defined rigid units noted for the Ag_3 and Zn_3 triangles here may be generalized to other systems. One can start by noting that each of the atoms in these triangles exhibit positive CPs directed roughly radially both into and away from the triangle center, creating quadrupolar CP distributions. In this case, transverse motions involving rotation of the unit appear as much easier than radial displacements. An examination of the CP schemes calculated earlier for structures with orientationally disordered clusters, such as the problematic tetrahedron in the Tsai-type approximant $CaCd_6$[57] or the $Fe@Al_{10}$ bicapped square antiprisms in $Fe_{14}Pd_{17}Al_{69}$,[58] affirms this theme. Conversely, anticipate disorder or soft phonon frequencies from rigid unit mode behavior in systems where groups of atoms are similarly enclosed in radially oriented CP quadrupoles. It would be interesting to explore how elemental substitution may modulate the orientations and order of such clusters, and, through these structural changes, influence the physical phenomena associated with the structures they occupy.

ASSOCIATED CONTENT

Supporting Information. Additional crystallographic information; data from WDS measurements; LDA-DFT optimized geometry of $Y_{14}Ag_{51}$; atomic coordinates for the Ag_3 triangles in the eclipsed and staggered models of $Y_{14}Ag_{51}$; electronic density of states distribution calculated for $Y_{14}Ag_{51}$; comparison of Ag_3 triangle CP features for the ground state, eclipsed, and staggered geometries for $Y_{14}Ag_{51}$. This material is available free of charge via the Internet at http://pubs.acs.org.

CSD 2383948 contains the supplementary crystallographic data for this Article. These data can be obtained free of charge from the Cambridge Crystallographic Database Centre via www.ccdc.cam.ac.uk/structures.

AUTHOR INFORMATION

Corresponding Author

* E-mail: rie.fredrickson@wisc.edu, danny@chem.wisc.edu

Author Contributions

The manuscript was written through contributions of all authors.

ACKNOWLEDGMENT

This Article is dedicated to the memory of Prof. Francis DiSalvo. We thank Dr. William O. Nachlas, Department of Geoscience, UW-Madison for WDS measurements. We gratefully acknowledge the financial support of the National Science Foundation through grant DMR-2127349.

REFERENCES

(1) Takakura, H.; Gómez, C. P.; Yamamoto, A.; De Boissieu, M.; Tsai, A. P. Atomic Structure of the Binary Icosahedral Yb-Cd Quasicrystal. *Nat. Mater.* **2007**, *6*, 58-63.

(2) Gómez, C. P.; Lidin, S. Comparative structural study of the disordered MCd_6 quasicrystal approximants. *Phys. Rev. B* **2003**, *68*, 024203.

(3) Piao, S. Y.; Gómez, C. P.; Lidin, S. Structural study of the disordered RECd6 quasicrystal approximants (RE = Tb, Ho, Er, Tm and Lu). *Z Naturforsch B* **2006**, *61*, 644-649.

(4) Widom, M.; Mihalkovič, M. Order-disorder transition in the Cd-Ca cubic approximant. *MRS Online Proceedings Library* **2003**, *805*, LL1.10.

(5) Lin, Q.; Corbett, J. D. $M_3(Au,Ge)_{19}$ and $M_{3.25}(Au,Ge)_{18}$ (M = Ca, Yb): Distinctive Phase Separations Driven by Configurational Disorder in Cubic YCd_6-Type Derivatives. *Inorg. Chem.* **2010**, *49*, 4570-4577.

(6) Popov, A. A.; Yang, S.; Dunsch, L. Endohedral Fullerenes. *Chem. Rev.* **2013**, *113*, 5989-6113.
(7) Rodríguez-Fortea, A.; Balch, A. L.; Poblet, J. M. Endohedral metallofullerenes: a unique host–guest association. *Chem. Soc. Rev.* **2011**, *40*, 3551-3563.
(8) Samson, S. The Crystal Structure of the Phase β-Mg_2Al_3. *Acta Crystallogr.* **1965**, *220*, 401-413.
(9) Feuerbacher, M.; Thomas, C.; Makongo, J. P. A.; Hoffmann, S.; Carrillo-Cabrera, W.; Cardoso, R.; Grin, Y.; Kreiner, G.; Joubert, J. M.; Schenk, T.; Gastaldi, J.; Nguyen-Thi, H.; Mangelinck-Noel, N.; Billia, B.; Donnadieu, P.; Czyrska-Filemonowicz, A.; Zielinska-Lipiec, A.; Dubiel, B.; Weber, T.; Schaub, P.; Krauss, G.; Gramlich, V.; Christensen, J.; Lidin, S.; Fredrickson, D.; Mihalkovic, M.; Sikora, W.; Malinowski, J.; Bruhne, S.; Proffen, T.; Assmus, W.; de Boissieu, M.; Bley, F.; Chemin, J. L.; Schreuer, J.; Steurer, W. The Samson Phase, *β*-Mg_2Al_3, Revisited. *Z.Kristallogr.* **2007**, *222*, 259-288.
(10) Montagné, P.; Tillard, M. Mg_2Al_3, a complex and disordered intermetallic compound as anode material for metal-air batteries. *J. Solid State Electrochem.* **2015**, *19*, 685-695.
(11) Fredrickson, R. T.; Fredrickson, D. C. Interface Nuclei in the Y–Ag–Zn System: Three Chemical Pressure-Templated Phases with Lamellar Mg_2Zn_{11}- and $CaPd_{5+x}$-Type Domains. *Inorg. Chem.* **2024**, *63*, 9252-9264.
(12) Tambornino, F.; Sappl, J.; Hoch, C. The $Gd_{14}Ag_{51}$ structure type and its relation to some complex amalgam structures. *J. Alloys Compd.* **2015**, *618*, 326-335.
(13) Lin, Q.; Corbett, J. D. $Ca_{14}Au_{46}Sn_5$: a "Colored" $Gd_{14}Ag_{51}$-Type Structure Containing Columns of Well-Differentiated Hexagonal Gold Stars. *Inorg. Chem.* **2011**, *50*, 1808-1815.
(14) Steeb, S.; Godel, D.; Löhr, C. On the structure of the compounds Ag_3R.E. (R.E. = Y, La, Ce, Sm, Gd, Dy, Ho, Er). *J. Less Common Met.* **1968**, *15*, 137-141.
(15) McMasters, O. D.; Gschneider, K. A., Jr; Venteicher, R. F. Crystallography of the silver-rich rare-earth-silver intermetallic compounds. *Acta Crystallogr. B* **1970**, *26*, 1224-1229.
(16) Haucke, W. Kristallstruktur von $CaZn_5$ und $CaCu_5$. *Z. Anorg. Allg. Chem.* **1940**, *244*, 17-22.
(17) Mühlpfordt, W. Zur Kenntnis des Systems Magnesium—Europium. IV. Die Kristallstruktur von Mg_5Eu. *Z. Anorg. Allg. Chem.* **1970**, *374*, 174-185.
(18) Mühlpfordt, W. Zur Kenntnis des Systems Magnesium-Europium. V. $(Eu_3Mg_{14})Mg_x$ mit $1{,}7 \le x \le 1$: Eine intermetallische Phase mit Kanalstruktur. *Z. Anorg. Allg. Chem.* **1997**, *623*, 985-989.
(19) Berns, V. M.; Fredrickson, D. C. Structural Plasticity: How Intermetallics Deform Themselves in Response to Chemical Pressure, and the Complex Structures That Result. *Inorg. Chem.* **2014**, *53*, 10762-10771.
(20) Kilduff, B. J.; Fredrickson, D. C. Chemical Pressure-Driven Incommensurability in $CaPd_5$: Clues to High-Pressure Chemistry Offered by Complex Intermetallics. *Inorg. Chem.* **2016**, *55*, 6781-6793.
(21) Dommann, A.; Hulliger, F. On the structure types of UAu_2 and $U_{14}Au_{51}$. *J. Less Common Met.* **1988**, *141*, 261-273.
(22) Celania, C.; Smetana, V.; Provino, A.; Manfrinetti, P.; Mudring, A.-V. $R_{14}(Au, M)_{51}$ (R = Y, La–Nd, Sm–Tb, Ho, Er, Yb, Lu; M = Al, Ga, Ge, In, Sn, Sb, Bi): Stability Ranges and Site Preference in the $Gd_{14}Ag_{51}$ Structure Type. *Cryst. Growth Des.* **2018**, *18*, 993-1001.
(23) Allibert, C.; Wong-Ng, W.; Nyburg, S. C. $CeCu_{3.6}$, a disordered variant of $Gd_{14}Ag_{51}$ type. *Acta Crystallogr. C* **1984**, *40*, 211-214.
(24) Belgacem, B.; Pasturel, M.; Tougait, O.; Potel, M.; Roisnel, T.; Ben Hassen, R.; Noël, H. Crystal structure and magnetic properties of novel intermetallic compounds in the Er–Cu–Ga system. *J. Alloys Compd.* **2009**, *478*, 89-95.
(25) Tkachuk, A. V.; Mar, A. Alkaline-Earth Metal Mercury Intermetallics $A_{11-x}Hg_{54+x}$ (A = Ca, Sr). *Inorg. Chem.* **2008**, *47*, 1313-1318.
(26) Hoch, C.; Simon, A. Na11Hg52: Complexity in a Polar Metal. *Angew. Chem. Int. Ed.* **2012**, *51*, 3262-3265.
(27) Tambornino, F.; Hoch, C. The Mercury-richest Europium Amalgam $Eu_{10}Hg_{55}$. *Z. Anorg. Allg. Chem.* **2015**, *641*, 537-542.
(28) Trovarelli, O.; Stickar, P.; Sereni, J. G.; Schmerber, G.; Kappler, J. P. Coexistence of magnetic and non magnetic states in $Ce_{14}X_{51}$ (X = Au, Ag and Cu). *Solid State Commun.* **1994**, *89*, 421-424.
(29) Schenck, A.; Pinkpank, M.; Gygax, F. N.; Neumann, K. U.; Ziebeck, K. R. A.; Amato, A. Magnetic properties of $U_{14}Au_{51}$: an exemplary study by muon spin-rotation spectroscopy. *J. Phys.: Condens. Matter* **1998**, *10*, 8059.
(30) Fischer, P.; Pomjakushin, V.; Keller, L.; Daoud-Aladine, A.; Sikora, W.; Dommann, A.; Hulliger, F. Antiferromagnetic three-sublattice Tb ordering in $Tb_{14}Ag_{51}$. *Phys. Rev. B* **2005**, *72*, 134413.
(31) Canepa, F.; Palenzona, A.; Eggenhöffner, R. Effects of the Th-substitution on the antiferromagnetic coupling and Kondo-like behaviour in the heavy-fermion system $U_{14}Au_{51}$. *Physica B: Condens. Matter* **1992**, *176*, 293-300.
(32) Kontani, M.; Nishioka, T.; Hamaguchi, Y.; Matsui, H.; Katori, H. A.; Goto, T. Magnetic Properties of Binary and Pseudobinary U-Au Heavy Fermion Systems. *J. Phys. Soc. Jpn.* **1994**, *63*, 3421-3430.
(33) Ghanta, S.; Häussermann, U.; Rydh, A. Synthesis, structure, and physical properties of a Y–Au-Ge 1/1 Tsai-type quasicrystal approximant and $Y_{14}(Au,Ge)_{51}$ with the $Gd_{14}Ag_{51}$ structure type. *J. Solid State Chem.* **2023**, *327*, 124246.
(34) Fredrickson, D. C. DFT-Chemical Pressure Analysis: Visualizing the Role of Atomic Size in Shaping the Structures of Inorganic Materials. *J. Am. Chem. Soc.* **2012**, *134*, 5991-5999.
(35) Engelkemier, J.; Fredrickson, D. C. Chemical Pressure Schemes for the Prediction of Soft Phonon Modes: A Chemist's Guide to the Vibrations of Solid State Materials. *Chem. Mater.* **2016**, *28*, 3171-3183.
(36) Hilleke, K. P.; Fredrickson, D. C. Discerning Chemical Pressure amidst Weak Potentials: Vibrational Modes and Dumbbell/Atom Substitution in Intermetallic Aluminides. *J. Phys. Chem. A* **2018**, *122*, 8412-8426.
(37) Sanders, K. M.; Van Buskirk, J. S.; Hilleke, K. P.; Fredrickson, D. C. Self-Consistent Chemical Pressure Analysis: Resolving Atomic Packing Effects through the Iterative Partitioning of Space and Energy. *J. Chem. Theory Comput.* **2023**, *19*, 4273-4285.
(38) Tao, J. Z.; Sleight, A. W. The role of rigid unit modes in negative thermal expansion. *J. Solid State Chem.* **2003**, *173*, 442-448.
(39) Hammonds, K. D.; Dove, M. T.; Giddy, A. P.; Heine, V.; Winkler, B. Rigid-unit phonon modes and structural phase transitions in framework silicates. *Am. Mineral.* **1996**, *81*, 1057-1079.
(40) Oszlányi, G.; Sütő, A. Ab initio structure solution by charge flipping. *Acta Crystallogr. Sect. A: Found. Crystallogr.* **2004**, *60*, 134-141.
(41) Oszlányi, G.; Sütő, A. Ab initio structure solution by charge flipping. II. Use of weak reflections. *Acta Crystallogr. Sect. A: Found. Crystallogr.* **2005**, *61*, 147-152.
(42) Palatinus, L.; Chapuis, G. SUPERFLIP - a computer program for the solution of crystal structures by charge flipping in arbitrary dimensions. *J. Appl. Crystallogr.* **2007**, *40*, 786-790.
(43) Petříček, V.; Palatinus, L.; Plášil, J.; Dušek, M. Jana2020 – a new version of the crystallographic computing system Jana. *Z. Kristallogr. - Cryst. Mater.* **2023**, *238*, 271-282.
(44) Gonze, X.; Rignanese, G.-m.; Verstraete, M.; Beuken, J.-m.; Pouillon, Y.; Caracas, R.; Raty, J.-y.; Olevano, V.; Bruneval, F.; Reining, L.; Godby, R.; Onida, G.; Hamann, D. R.; Allan, D. C. A Brief Introduction to the ABINIT Software Package. *Z. Kristallogr.* **2005**, *220*, 558-562.
(45) Gonze, X.; Amadon, B.; Anglade, P.-M.; Beuken, J.-M.; Bottin, F.; Boulanger, P.; Bruneval, F.; Caliste, D.; Caracas, R.; Côté, M.; Deutsch, T.; Genovese, L.; Ghosez, P.; Giantomassi, M.; Goedecker, S.; Hamann, D. R.; Hermet, P.; Jollet, F.; Jomard, G.; Leroux, S.; Mancini, M.; Mazevet, S.; Oliveira, M. J. T.; Onida, G.; Pouillon, Y.; Rangel, T.; Rignanese, G.-M.; Sangalli, D.; Shaltaf, R.; Torrent, M.; Verstraete, M. J.; Zerah, G.; Zwanziger, J. W. ABINIT: First-principles Approach to Material and Nanosystem Properties. *Comput. Phys. Commun.* **2009**, *180*, 2582-2615.
(46) Hartwigsen, C.; Goedecker, S.; Hutter, J. Relativistic Separable Dual-space Gaussian Pseudopotentials from H to Rn. *Phys. Rev. B* **1998**, *58*, 3641-3662.
(47) Berns, V. M.; Engelkemier, J.; Guo, Y.; Kilduff, B. J.; Fredrickson, D. C. Progress in Visualizing Atomic Size Effects with DFT-Chemical Pressure Analysis: From Isolated Atoms to Trends in AB_5 Intermetallics. *J. Chem. Theory Comput.* **2014**, *10*, 3380-3392.
(48) Oliveira, M. J. T.; Nogueira, F. Generating relativistic pseudo-potentials with explicit incorporation of semi-core states using APE, the Atomic Pseudo-potentials Engine. *Comput. Phys. Commun.* **2008**, *178*, 524-534.
(49) Engelkemier, J.; Berns, V. M.; Fredrickson, D. C. First-Principles Elucidation of Atomic Size Effects Using DFT-Chemical Pressure Analysis: Origins of $Ca_{36}Sn_{23}$'s Long-Period Superstructure. *J. Chem. Theory Comput.* **2013**, *9*, 3170-3180.
(50) Fredrickson, R. T.; Kamp, K. R.; Fredrickson, D. C. Local Stability to Periodicity in the $EuMg_{5+x}$ Type: Chemical Pressure, Disordered Channels, and

Predicted Superstructure in $YZn_{5.225}$. *Z. Anorg. Allg. Chem.* **2022**, *648*, e202200068.
(51) Okamoto, H. Ag-Zn (Silver-Zinc) In *Binary Alloy Phase Diagrams, 2nd Ed.*; Massalski, T. B., Ed.; ASM International: Materials Park, Ohio, 1990, p 117-118.
(52) Bergerhoff, G.; Brown, I. D. Inorganic Crystal Structure Database In *Crystallographic Databases*; Allen, F. H., Bergerhoff, Sievers, R., Eds.; International Union of Crystallography: Chester, 1987, p 77-95.
(53) Belsky, A.; Hellenbrandt, M.; Karen, V. L.; Luksch, P. New developments in the Inorganic Crystal Structure Database (ICSD): accessibility in support of materials research and design. *Acta Crystallogr. B* **2002**, *58*, 364-369.
(54) Pettifor, D. G. *Bonding and Structure of Molecules and Solids*; Oxford University Press: Oxford, 1995.
(55) Hilleke, K. P.; Fredrickson, R. T.; Vinokur, A. I.; Fredrickson, D. C. Substitution Patterns Understood through Chemical Pressure Analysis: Atom/Dumbbell and Ru/Co Ordering in Derivatives of YCo_5. *Cryst. Growth Des.* **2017**, *17*, 1610-1619.
(56) Gómez, C. P.; Lidin, S. Superstructure of Eu_4Cd_{25}: A quasicrystal approximant. *Chem. Eur. J.* **2004**, *10*, 3279-3285.
(57) Berns, V. M.; Fredrickson, D. C. Problem Solving with Pentagons: Tsai-Type Quasicrystal as a Structural Response to Chemical Pressure. *Inorg. Chem.* **2013**, *52*, 12875-12877.
(58) Peterson, G. G. C.; Yannello, V. J.; Fredrickson, D. C. Inducing Complexity in Intermetallics through Electron–Hole Matching: The Structure of $Fe_{14}Pd_{17}Al_{69}$. *Angew. Chem. Int. Ed.* **2017**, *56*, 10145-10150.

For Table of Contents Use Only

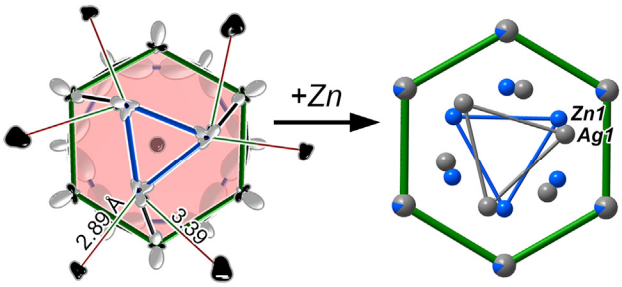

$Y_{14}Ag_{51}$ CP scheme $Y_{14}Ag_{39.3}Zn_{12.1}$